Giant and Broad-Band Absorption Enhancement in Colloidal Quantum Dot Monolayers through Dipolar Coupling

Pieter Geiregat,[†,‡,§] Yolanda Justo,[†,§] Sofie Abe,[†,§] Stijn Flamee,[†,§] and Zeger Hens[†,§,*]

[†]Physics and Chemistry of Nanostructures, [‡]Photonics Research Group, and [§]Center for Nano and Biophotonics, Ghent University, B-9000 Ghent, Belgium

ABSTRACT The absorption cross section of colloidal quantum dots in close-packed monolayers shows a 4 (CdSe) to 5-fold (PbS) enhancement compared to quantum dots in a dilute dispersion. Quantitative agreement is demonstrated between the value and the size dependence of the enhancement and theoretical model predictions based on dipolar coupling between neighboring quantum dots. This collective optical behavior offers a new degree of freedom in the custom design of optical properties for electro-optical devices.

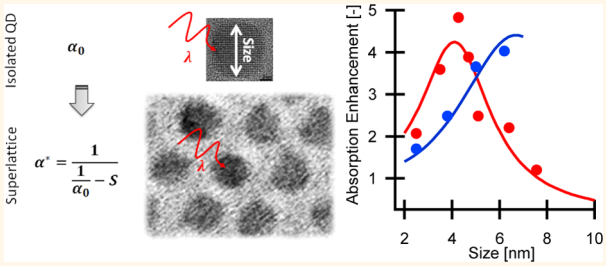

KEYWORDS: nanocrystals · superlattice · optical properties · light absorption · coupled dipole model

Like atoms forming macroscopic crystals, nanoparticle superlattices (NSLs) can exhibit physical properties different from their individual constituents.[1] These properties can be tuned by means of the characteristics of the building blocks (size, shape, ferromagnetic, metallic, *etc.*), the lattice structure (particle separation, lattice symmetry, *etc.*), or the interparticle interactions (electromagnetic and/or quantum mechanical coupling, *etc.*). Lithographically defined arrays of metallic nanoparticles, for example, show collective optical properties based on coupling through near-field and/or long-range dipolar interactions which strongly affect the single-particle plasmon resonance.[2,3] Similarly, long-range electromagnetic interactions have recently been observed in ensembles of epitaxially grown, semiconducting quantum dots.[4] However, both the plasmonic and the epitaxial systems are limited by their fabrication process, which prevents the formation of heterogeneous superlattices or assemblies with high packing densities. An alternative to these lithography-based techniques is the bottom-up formation of NSLs by self-assembly of colloidal nanocrystals. These nanometer-sized metal, metal oxide, or semiconductor crystals are synthesized with low size dispersion by a solution-based synthesis.[5] Single-component, binary, and even ternary close-packed NSLs have been demonstrated,[1,6−8] in which crucial parameters such as the type of building block, the interparticle spacing, and the superlattice symmetry can be adjusted. Although colloidal NSLs are of great fundamental and practical interest, few collective physical properties resulting from coupling between nanocrystals have been demonstrated so far because NSLs are difficult to make over large areas. Using a more simple one-component, two-dimensional (2D) array of PbSe quantum dots (QDs), electronic coupling has been demonstrated by means of scanning tunneling spectroscopy.[9] In the case of binary NSLs, single-phase-like magnetization was observed with differently sized Fe_3O_4 nanocrystals and attributed to magnetic dipole coupling.[10]

Here, we analyze the absorption cross section (σ_f) of PbS and CdSe QDs in close-packed one-component monolayers.[11,12] These materials have been chosen since CdSe is the most widely used colloidal QD and, as such, a reference material, while PbS QDs hold great promise for photovoltaics and infrared photodetection,[13,14] applications where light absorbance is a key material property.

* Address correspondence to zeger.hens@ugent.be.

Received for review July 11, 2012 and accepted January 8, 2013.

Published online January 08, 2013
10.1021/nn305524a

Compared to literature data on the absorption cross section in diluted dispersions ($\sigma_{0,s}$) of both materials, we find that σ_f can be enhanced up to a factor of 4 (CdSe) or 5 (PbS). For example, in the case of PbS QDs, the enhancement $\mathcal{E} = \sigma_f/\sigma_{0,s}$ shows a marked, resonance-like diameter dependence, with a maximum value for QDs of around 4 nm. Similar results are obtained for CdSe. We also show a strong dependence on the superlattice parameters by studying the effect of the interparticle spacing on fixed size CdSe nanocrystals. Moreover, $\mathcal{E}$ is largely wavelength-independent, which was validated for PbS. We show that the value and the layer parameter dependence of $\mathcal{E}$ for both PbS and CdSe can be quantitatively described by considering the dipolar coupling between neighboring QDs in the close-packed film. According to this description, the resonance behavior results from the condition for optimal coupling, where the mutual enhancement of the electric fields of neighboring QDs is maximized. In this way, we demonstrate that light absorption by a close-packed film of quantum dots is a joint property of the individual QDs and the QD superlattice, thereby showing for the first time a truly collective optical effect in colloidal nanocrystal superlattices.

RESULTS

This work makes use of monodispersed batches of CdSe and PbS QDs stabilized by carboxylate ligands. They have been synthesized following literature recipes, with diameters d_{QD} ranging from 2.5 to 6.2 nm for CdSe and 2.5 to 8 nm for PbS (see Methods). In both cases, QD monolayers are formed by spreading a QD dispersion on a Langmuir trough, followed by the transfer of the Langmuir film to a glass substrate using Langmuir–Blodgett deposition. As shown in Figure 1, this results in homogeneous monolayers over square centimeter areas, with typical surface coverages as determined by atomic force microscopy (AFM) of 95% or more. In addition, transmission electron microscopy (TEM) demonstrates that the monolayers have a locally hexagonal ordering. The QD surface density (N_s) is determined from TEM micrographs (Figure 1c), while the QD interdistance—written as $d_{QD} + 2l$, where l denotes the thickness of the ligand shell—is obtained from more detailed TEM analysis (see Figure 1d). The absorption cross section σ_f of a QD in these close-packed monolayers is calculated from the absorbance A and the reflectance R:

$$\sigma_f = \ln 10 \times \frac{A - R}{N_s} \qquad (1)$$

In this expression, scattering is neglected since the wavelengths used (>335 nm) are much larger than the quantum dot diameter. The correction of the absorbance for reflection is typically very small (<10%) (see Supporting Information, section 2). To calculate the absorption enhancement, we combine the experimental

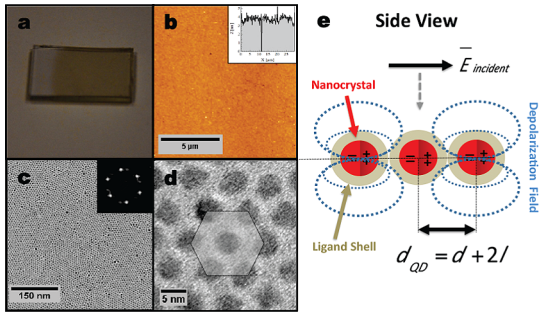

Figure 1. Langmuir–Blodgett monolayer of PbS quantum dots. (a) Contrast picture of a monolayer of PbS quantum dots (d = 5 nm) on a glass surface (2 cm × 1 cm) showing homogeneous cm^2 coverage. (b) Atomic force microscope scan of the same PbS monolayer indicating excellent area uniformity (inset: cross section). (c) Larger area TEM image showing the PbS quantum dot superlattice with local hexagonal ordering (inset: Fourier transform image). (d) Zoomed-in TEM image showing the individual quantum dots and their interdistance. (e) Side view schematic of monolayer subject to incident field polarized in-plane. The relevant geometrical parameters are indicated by d_{QD}, d, and l as the (nearest-neighbor) interdot distance, QD size, and ligand length, respectively.

values of σ_f with published values[15,16] for $\sigma_{0,s}$, where we work at 400 nm for PbS and at 335 nm for CdSe.

Figure 2a,b shows the absorption enhancement $\mathcal{E}$ for PbS and CdSe QDs stabilized by oleate ligands as a function of their diameter at 400 and 335 nm, respectively. For PbS, we find that $\mathcal{E}$ initially increases with increasing particle size up to a maximum of 5 at a core size of around 4 nm. For larger sizes, $\mathcal{E}$ decreases and reaches values of about 1 for 8 nm particles. In the case of CdSe, $\mathcal{E}$ steadily increases within the diameter range studied to level off at a value of around 4 for a diameter of 6.2 nm. We also investigated the influence of the thickness of the ligand shell l. In particular, for a fixed size of CdSe nanocrystal (4.4 nm), the ligand shell was exchanged from oleate to shorter chain carboxylates, including palmitate (C16), myristate (C14), and laureate (C12). Figure 2 represents the enhancement as a function of the ligand length—as determined from TEM analysis—thus obtained. We find that $\mathcal{E}$ steadily decreases from a value of 4 in the case of laureate ligands (l = 1.1 nm) to a value of around 2 for oleate ligands (l = 1.5 nm).

DISCUSSION

Enhancement within the Maxwell–Garnett Effective Medium Theory. To analyze the enhancement of σ_f relative to $\sigma_{0,s}$, including its remarkable diameter and ligand length dependence, we start from the fact that light absorption by isolated QDs can be understood within the framework of the Maxwell–Garnett effective medium theory. This yields an absorption cross section $\sigma_{0,s}$ given by

$$\sigma_{0,s} = V_{QD}\frac{2\pi}{\lambda n_s}\frac{9\varepsilon_s^2}{|\varepsilon_{QD}+2\varepsilon_s|^2}\,\mathrm{Im}(\varepsilon_{QD}) \qquad (2)$$

where V_{QD} is the QD volume; n_s is the refractive index of the solvent; ε_s is the dielectric constant of the solvent at

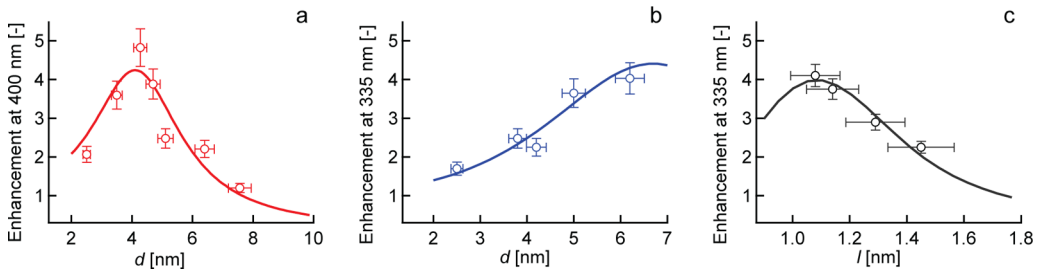

Figure 2. Absorption enhancement $\mathcal{E}$ for (a) PbS quantum dots stabilized by oleate ligands (l = 1.5 nm) at 400 nm as a function of QD diameter d; (b) CdSe quantum dots stabilized by oleate ligands (l = 1.5 nm) at 335 nm as a function of d; and (c) CdSe quantum dots (d = 4.4 nm) as a function of ligand length l, where the respective data points have been obtained using laureate, myristate, palmitate, and oleate ligands.

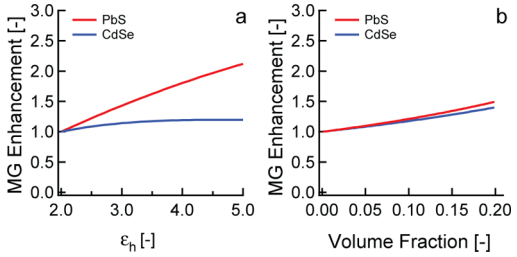

Figure 3. Absorption enhancement $\mathcal{E}$ in the Maxwell–Garnett (MG) model for (a) increasing dielectric constant of the particle environment at a fixed volume fraction and (b) *vice versa*.

the radiation frequency; and ε_{QD} is the dielectric function of the QD materials at the radiation frequency.

Typically, $|\varepsilon_{QD}|$ strongly exceeds $|\varepsilon_s|$ for QDs dispersed in an apolar, organic solvent, a condition implying that the optical electric field in the QDs is strongly screened. An increase of $|\varepsilon_s|$ and the concomitant reduction of this screening will therefore result in an enhancement of the absorption cross section (see eq 2). Hence, a first possible origin of the enhanced absorption of QDs in a close-packed thin film is the reduced screening of the incident light by an increase of the dielectric constant of the environment. This increase could, for example, be due to the presence of neighboring particles in the film or due to the presence of the glass substrate. However, as is shown in Figure 3a, not only is this effect size-independent but it also fails to account for the large enhancements up to 5 measured experimentally. A similar conclusion is arrived at when explicitly taking the volume fraction of the absorbers into account in the Maxwell–Garnett expression for a given host permittivity (see Figure 3b).[17] This indicates that the Maxwell–Garnett mixing rule breaks down in films of close-packed nanocrystals.

Coupled Dipole Model. An alternative approach to derive eq 2 is to see each QD as a polarizable point particle with a polarizability $\alpha_{0,s}$ that depends on its volume, ε_{QD} and ε_s:

$$\alpha_{0,s} = 4\pi\varepsilon_0 r^3 \varepsilon_s \frac{\varepsilon_{QD} - \varepsilon_s}{\varepsilon_{QD} + 2\varepsilon_s} \quad (3)$$

Equation 2 is then recovered by the relation between the absorption cross section and the imaginary part of $\alpha_{0,s}$ (see Supporting Information):

$$\sigma_{0,s} = \frac{2\pi}{\lambda n_s} \mathrm{Im}(\alpha_{0,s}) \quad (4)$$

Describing QDs as polarizable point particles, the exceptional absorption enhancement in close-packed QD monolayers can be intuitively understood by means of dipolar coupling between neighboring QDs. A polarized QD will induce a polarization field with dominant dipolar character,[18] decaying rapidly outside of the QD. However, opposite from isolated QDs (*e.g.*, in a dilute solution), neighboring QDs in a close-packed layer will feel this additional field. Hence, their polarization by an external driving field will be different from that of an isolated QD, which results in a change in absorption cross section. Since the distance d_{ij} between two dipoles i and j in a close-packed film increases linearly with the QD radius, there is a trade-off in this dipolar coupling: larger particles show a larger polarizability but increased interparticle spacing. Apparently, this gives rise to an optimal separation or, equivalently, an optimal particle size for dipolar coupling, as follows from the experimental data in Figure 2.

This qualitative description can be quantified by the coupled dipole (CD) model, which was originally developed to explain collective resonance effects in arrays of metallic particles.[2,3,19] Such particles show distinct multipolar plasmon resonances in their single-particle polarizability, thus differing fundamentally from the semiconducting QDs studied here. Within this model, we write the local field $E_{L,i}$ polarizing a particular QD i as the sum of the incident external field E and the contribution from the polarization fields of all other QDs j:

$$E_{L,i} = E + \sum_{j \neq i} \beta_{i,j} E_{L,j} \quad (5)$$

Here, the coupling coefficients $\beta_{i,j}$ describe the dipole field of QD j at the position of QD i. They are thus proportional to $\alpha_{0,h}/\varepsilon_h$, that is, the polarizability of an individual QD screened by the host. More importantly, due to symmetry reasons, all QDs must experience the same local field E_L. Thus, we can rewrite eq 5 as

$$E_L = E + \frac{\alpha_{0,h}}{\varepsilon_h} \sum_{j \neq i} S_{i,j} E_L = E + \frac{\alpha_{0,h}}{\varepsilon_h} S E_L \quad (6)$$

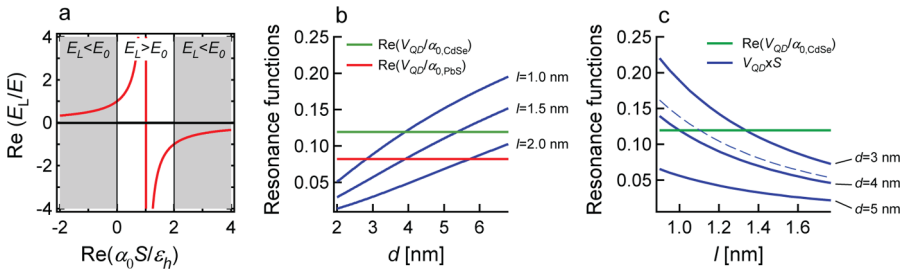

Figure 4. (a) Ratio of the local driving field E_L and the external driving field E as a function of the coupling between neighboring QDs as expressed by eq 8. (b) Graphical representation of the optimal coupling condition (eq 9) showing the term $\varepsilon_h V_{QD}/\alpha_{0,h}$ for (red) PbS QDs at 400 nm and (green) CdSe QDs at 335 nm, together with the term (blue) $V_{QD}S$ for ligand lengths l as indicated as a function of particle size. (c) Same terms plotted as a function of ligand length l for different particle sizes as indicated. In (b) and (c), optimal coupling for a given material and a given size or ligand length corresponds to the crossing of the respective horizontal and blue lines. Calculations are done taking $\varepsilon_h = 1.5$ and assuming local hexagonal ordering in the monolayers.

The quantity S, introduced in eq 6, is called the retarded dipole sum. It includes the dipolar contributions from all neighboring particles to the internal field of the considered particle. As outlined in the Supporting Information, a simplified expression for S is obtained by assuming that image charges induced in the substrate are negligible due to its low permittivity, that the center-to-center distance d_{ij} between neighboring QDs is small compared to the optical wavelength $\lambda = 2\pi/k$, and that the monolayers show only locally hexagonal ordering:

$$S = \sum_{j \neq i} \frac{(1 - kd_{ij})e^{ikd_{ij}}}{8\pi d_{ij}^3} \qquad (7)$$

Rewriting eq 6, we obtain an expression for the field locally driving an individual QD as a function of the incident electric field:

$$E_L = \frac{E}{1 - \frac{\alpha_{0,h}}{\varepsilon_h} S} \qquad (8)$$

Equation 8, which describes the local driving field E_L as a function of the incident field E, provides an excellent starting point to understand the occurrence of a maximum enhancement. It indicates that the ratio between E_L and E crucially depends on the product $\alpha_{0,h}S/\varepsilon_h$, that is, on the combination of the polarizability of an individual QD and the coupling between the QDs. On the basis of the respective definitions of $\alpha_{0,h}$ and S, it follows that this quantity changes depending on the QD material, the driving frequency (*via* ε_{QD}), the diameter of the QDs, and the distance between neighboring QDs. Assuming for simplicity that $\alpha_{0,h}S/\varepsilon_h$ is a real number, E_L will be enhanced relative to E when $0 < \alpha_{0,h}S/\varepsilon_h < 2$ (see Figure 4a). Moreover, E_L increases to infinity when $\alpha_{0,h}S/\varepsilon_h = 1$. Returning to eq 6, this actually means that the system of dipoles can support a local driving field without external driving field at the particular driving frequency where this condition holds. Hence, the condition $\alpha_{0,h}S/\varepsilon_h = 1$ determines a resonance condition for the 2D array of coupled, oscillating dipoles. Obviously, we expect that around this resonance condition the absorbance of the layer will be maximally enhanced, a situation we call optimal coupling. We note that neglecting the imaginary part of the denominator in eq 8 is useful for understanding the resonance condition. In reality, the imaginary part limits the increase of E_L, resulting in a damped resonance. For a quantitative comparison between the experimental results and the theory developed here, both the real and imaginary part of S and $\alpha_{0,h}$ are to be taken into account.

Dependence of the Enhancement on Nanocrystal Size and Ligand Length. In the experiments shown in Figure 2, we fix the driving frequency—and thus ε_{QD}—yet we change $\alpha_{0,h}$ *via* the QD size and S *via* both the QD size and the ligand length. To analyze the occurrence of optimal coupling in this case, we rewrite the resonance condition as

$$\frac{\varepsilon_h \times V_{QD}}{\alpha_{0,h}} = V_{QD} \times S \qquad (9)$$

In eq 9, the left-hand side depends on the QD material and the driving frequency but not on the QD size or the interparticle spacing. On the other hand, the right-hand side depends on the geometrical parameters of the close-packed layer (*i.e.*, d_{QD} and l). By varying d_{QD} or l, we thus only change ($V_{QD} \times S$), and optimal coupling occurs when eq 9 holds. When $l = 1.5$ nm—the experimentally determined ligand shell thickness in the Langmuir–Blodgett films of QDs capped with oleate ligands—Figure 4b shows that this results in optimal coupling for ≈4 nm PbS QDs. This value matches the experimentally observed diameter for maximum enhancement, confirming that the mutual dipolar coupling between adjacent QDs indeed accounts for the observed absorption enhancement. Equation 9 and Figure 4b also show that the lower polarizability of CdSe QDs means that larger diameters are needed to reach optimal coupling, which is also confirmed experimentally (see Figure 2b). Also, the dependence of the resonance on ligand length can be understood

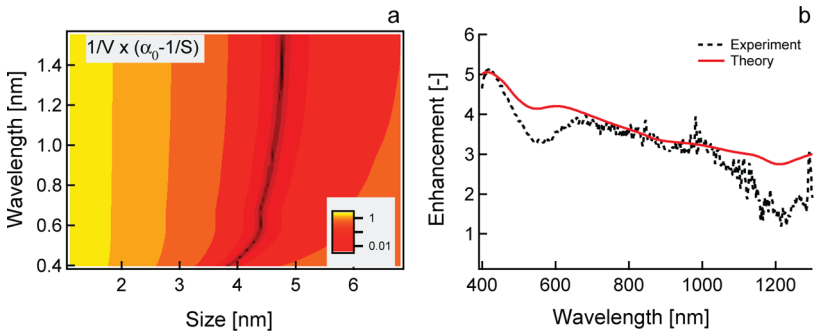

Figure 5. (a) Plot of $(\alpha_{0,h}/\varepsilon_h - 1/S)/V$ as a function of QD diameter and wavelength according to the indicated color code. Optimal coupling corresponds to a value of 0, indicated as dark brown ($\varepsilon_h = 1.5$). (b) Spectrum of the absorption enhancement as (black) measured and (red) calculated for 4.3 nm PbS QDs.

using the resonance condition described in eq 9. As plotted in Figure 4c, optimal coupling for 4.4 nm CdSe QDs occurs for a ligand length close to 1.1 nm, which implies a progressive reduction of $\mathcal{E}$ for ligand lengths that progressively exceed this value, in line with the experimental data in Figure 2c.

For a more quantitative comparison between our experimental data and the coupled dipole model, we use eq 8 to obtain an effective polarizability α_{film} of a QD in a close-packed monolayer (see Supporting Information, section 1.3−1.4):

$$\alpha_{film} = \frac{\alpha_{0,h}}{1 - \frac{\alpha_{0,h}}{\varepsilon_h} S} \tag{10}$$

As a result, σ_f and the absorption enhancement read

$$\sigma_f = \frac{2\pi}{\lambda n_h} \mathrm{Im}\left(\frac{\alpha_{0,h}}{1 - \frac{\alpha_{0,h}}{\varepsilon_h} S} \right) \tag{11}$$

$$\mathcal{E} = \frac{\sigma_f}{\sigma_{0,s}} = \frac{n_s}{n_h} \frac{\mathrm{Im}\left(\frac{\alpha_{0,h}}{1 - \frac{\alpha_{0,h}}{\varepsilon_h} S} \right)}{\mathrm{Im}(\alpha_{0,s})} \tag{12}$$

Equation 12 shows that the condition for optimal coupling also controls the enhancement of σ_f. In Figure 2, the solid lines represent $\mathcal{E}$ for PbS and CdSe QDs, calculated using eq 12 at 400 and 335 nm, respectively. As is common for the high-energy dielectric function of semiconductor quantum dots, the respective bulk values are used for ε_{QD}. In addition, the film environment is modeled as $\varepsilon_h = 1.5$, which corresponds to an environment of low polarizability. This is a reasonable estimate for an environment consisting of organic ligands, glass, and air. Assuming a size dispersion of 10%, we find that the experimental enhancement is in very good agreement with the enhancement that follows from the assumption of dipolar coupling between neighboring QDs. For both PbS and CdSe, the magnitude and the size dependence of $\mathcal{E}$ are correctly predicted with, for the particular example of PbS, a maximum enhancement for a diameter of around 4 nm. Also, for CdSe, the dependence of $\mathcal{E}$ on the ligand length l is well reproduced.

Wavelength Dependence of the Enhancement. In Figure 2a, we pass through the condition of optimal coupling by changing d_{QD}. Alternatively, optimal coupling could also be obtained by changing the wavelength λ of the incident light. The color scale in Figure 5a shows the optimal coupling condition—as determined by eq 9—as a function of both variables. While changing d_{QD} results in a relatively narrow resonance, one sees that the condition for optimal coupling hardly depends on λ. This minor wavelength dependence can be understood from the nonresonant polarizability of individual QDs in the wavelength range considered. Opposite from metal nanocrystals driven near their surface plasmon resonance, this leads to a limited change of α_0. Importantly, this implies that, for a fixed QD diameter, the absorption will be enhanced over a broad wavelength range. This prediction is confirmed by the spectrum of $\mathcal{E}$ for 4.3 nm PbS QDs as represented in Figure 5b, where $\mathcal{E}$ decreases gradually from a value of 5 around 400 nm to 3 around 1000 nm. This overall trend is well reproduced by the coupled dipole model, where we now use the frequency-dependent dielectric function of PbS nanocrystals as obtained through the Kramers−Krönig relations.[20] Nanocrystal devices for photodetection or solar energy conversion typically face a trade-off between light absorption, which improves with thicker layers, and charge carrier extraction, where thinner films are preferred. Hence, the possibility to enhance the absorption over a broad wavelength range by tuning the nanocrystal size and the inter-nanocrystal spacing is very relevant for these applications.

CONCLUSION

In summary, we have demonstrated strong optical coupling phenomena in close-packed monolayers of colloidal QDs, leading to giant enhancement of the absorbance per QD up to a factor of 5. The results can be explained and quantified using a dipolar coupling model. On top of the cheap bottom-up fabrication and processing, a collective property such as absorption enhancement makes colloidal QDs extremely suited

for applications in photovoltaics and photodetection, where a trade-off between layer thickness and light absorption restricts conversion efficiencies. The model presented here provides a general framework to further study the optical properties of the simple, single-component superlattices analyzed here, where possible open questions are the difference between s- and p-polarized light and the impact optimal coupling has on the radiative lifetime. Moreover, it gives a basis to understand the optical properties of more complex, possibly hybrid superlattices, for example, containing nanocrystals of different sizes or different materials.

METHODS

Materials. Oleylamine (OLA)-capped PbS QDs were synthesized using the procedure described by Cademartiri *et al.*[21] and modified by Moreels *et al.*[22] After synthesis, the OLA ligand shell is substituted by oleic acid (OA). An exchange to OA is typically performed by adding OA to a toluene suspension of PbS QDs in a ratio of 1.5:10 OA/toluene. After precipitation with EtOH and centrifugation, the QDs are resuspended in toluene and the exchange is repeated. Oleate-capped CdSe QDs were synthesized according to the procedure developed by Jasieniak *et al.*[23] CdSe QDs with a diameter of 6.2 nm were prepared using a similar synthesis combined with the controlled injection of additional precursors. After 40 min of synthesis, we slowly inject a mixture of precursors and solvent with the same composition as the initial reaction mixture during 50 min. Next, the reaction is allowed to continue for an additional 1 h before the mixture is cooled to room temperature and purified.

Ligand Exchange. Ligand exchange was carried out on 4.4 nm CdSe QDs capped with oleic acid. As substitute ligands (SL), we used carboxylic acids with different chain lengths from palmitic acid (C16) to lauric acid (C12). A ligand exchange is typically performed by adding an excess of the SL to a toluene suspension of CdSe QDs in a molar ratio of 200:1 SL/OA. After precipitation with methanol (MeOH) and centrifugation, the QDs are resuspended in toluene. The exchange is repeated three times to ensure full exchange. Finally, the QDs are precipitated one more time with MeOH to remove any excess of the SL.

Layer Formation. To produce QD monolayers, we spread the QDs dissolved in chloroform on a water surface using a commercial Langmuir–Blodgett trough (Nima 310).The monolayers are transferred at a surface pressure of 12–30 mN/m to glass substrates by Langmuir–Blodgett deposition or to TEM grids by Langmuir–Schaeffer deposition.

Absorbance Measurements. The absorption and reflection of the monolayers is measured using a commercial spectrophotometer (Perkin-Elmer Lambda 950 UV–vis–NIR) equipped with an absolute reflectance measurement (URA) tool. Typically, three (absolute, *i.e.*, no reference recorded before) spectra are recorded (both for absorption and reflection): an internal (instrument related) calibration, a bare glass sample, and the glass sample covered with the monolayer under study. The quantities A and R are then obtained through subsequent subtraction procedures. Such procedures are valid for thin films where interference effects can be neglected. This method provided us with the best accuracy for weakly absorbing and reflecting samples.

Conflict of Interest: The authors declare no competing financial interest.

Acknowledgment. This research is funded by Ghent University (Special Research Fund), the FWO-Vlaanderen (G.0760.12, G.0794.10), BelSPo (IAP 7.35, photonics@be), and EU-FP7 (Navolchi).

Supporting Information Available: Full mathematical description of the adapted coupled dipole model and a description of the reflectance correction and TEM analysis. This material is available free of charge *via* the Internet at http://pubs.acs.org.

REFERENCES AND NOTES

1. Talapin, D. V.; Shevchenko, E. V.; Bodnarchuk, M. I.; Ye, X.; Chen, J.; Murray, C. B. Quasicrystalline Order in Self-Assembled Binary Nanoparticle Superlattices. *Nature* **2009**, *461*, 964–967.
2. Jensen, T.; Kelly, L.; Lazarides, A.; Schatz, G. C. Electrodynamics of Noble Metal Nanoparticles and Nanoparticle Clusters. *J. Cluster Sci.* **1999**, *10*, 295–317.
3. Zhao, L.; Kelly, K. L.; Schatz, G. C. The Extinction Spectra of Silver Nanoparticle Arrays: Influence of Array Structure on Plasmon Resonance Wavelength and Width. *J. Phys. Chem. B* **2003**, *107*, 7343–7350.
4. Bogaart, E. W.; Haverkort, J. E. M. Anomalous Exciton Lifetime by Electromagnetic Coupling of Self-Assembled InAs/GaAs Quantum Dots. *J. Appl. Phys.* **2010**, *107*, 064313.
5. Yin, Y.; Alivisatos, P. Colloidal Nanocrystal Synthesis and the Organic–Inorganic Interface. *Nature* **2005**, *437*, 664–670.
6. Shevchenko, E. V.; Talapin, D. V.; Kotov, N. A.; O'Brien, S.; Murray, C. B. Structural Diversity in Binary Nanoparticle Superlattices. *Nature* **2006**, *439*, 55–59.
7. Dong, A.; Ye, X.; Chen, J.; Murray, C. B. Two-Dimensional Binary and Ternary Nanocrystal Superlattices: The Case of Monolayers and Bilayers. *Nano Lett.* **2011**, 1804–1809.
8. Talapin, D. V.; Shevchenko, E. V.; Murray, C. B.; Titov, A. V.; Kral, P. Dipole–Dipole Interactions in Nanoparticle Superlattices. *Nano Lett.* **2007**, *7*, 1213–1219.
9. Overgaag, K.; Liljeroth, P.; Grandidier, B.; Vanmaekelbergh, D. Scanning Tunneling Spectroscopy of Individual PbSe Quantum Dots and Molecular Aggregates Stabilized in an Inert Nanocrystal Matrix. *ACS Nano* **2008**, *2*, 600–606.
10. Chen, J.; Dong, A.; Cai, J.; Ye, X.; Kang, Y.; Kikkawa, J. M.; Murray, C. B. Collective Dipolar Interactions in Self-Assembled Magnetic Binary Nanocrystal Superlattice Membranes. *Nano Lett.* **2010**, *10*, 5103–5108.
11. Justo, Y.; Moreels, I.; Lambert, K.; Hens, Z. Langmuir–Blodgett Monolayers of Colloidal Lead Chalcogenide Quantum Dots: Morphology and Photoluminescence. *Nanotechnology* **2010**, *21*, 295606.
12. Lambert, K.; Capek, R. K.; Bodnarchuk, M. I.; Kovalenko, M. V.; Van Thourhout, D.; Heiss, W.; Hens, Z. Langmuir–Schaefer Deposition of Quantum Dot Multilayers. *Langmuir* **2010**, *26*, 7732–7736.
13. Sargent, E. H. Infrared Photovoltaics Made by Solution Processing. *Nat. Photonics* **2009**, *3*, 325–331.
14. Clifford, J. P.; Konstantatos, G.; Johnston, K. W.; Hoogland, S.; Levina, L.; Sargent, E. H. Fast, Sensitive and Spectrally Tuneable Colloidal-Quantum-Dot Photodetectors. *Nat. Nanotechnol.* **2009**, *4*, 40–44.
15. Moreels, I.; Lambert, K.; Smeets, D.; De Muynck, D.; Nollet, T.; Martins, J. C.; Vanhaecke, F.; Vantomme, A.; Delerue, C.; Allan, G.; *et al.* Size-Dependent Optical Properties of Colloidal PbS Quantum Dots. *ACS Nano* **2009**, *3*, 3023–3030.
16. Capek, R. K.; Moreels, I.; Lambert, K.; De Muynck, D.; Zhao, Q.; Van Tomme, A.; Vanhaecke, F.; Hens, Z. Optical Properties of Zincblende Cadmium Selenide Quantum Dots. *J. Phys. Chem. C* **2010**, *114*, 6371–6376.
17. Hens, Z.; Moreels, I. Light Absorption by Colloidal Semiconductor Quantum Dots. *J. Mater. Chem.* **2012**, *22*, 10406–10415.
18. Jackson, J. *Classical Electrodynamics*, 3rd ed.; Wiley: New York, 1999.
19. Haynes, C. L.; McFarland, A. D.; Zhao, L.; Van Duyne, R. P.; Schatz, G. C.; Gunnarsson, L.; Prikulis, J.; Kasemo, B.; Käll, M. Nanoparticle Optics: The Importance of Radiative Dipole Coupling in Two-Dimensional Nanoparticle Arrays. *J. Phys. Chem. B* **2003**, *107*, 7337–7342.

20. Moreels, I.; Allan, G.; De Geyter, B.; Wirtz, L.; Delerue, C.; Hens, Z. Dielectric Function of Colloidal Lead Chalcogenide Quantum Dots Obtained by a Kramers−Krönig Analysis of the Absorbance Spectrum. *Phys. Rev. B* **2010**, *81*, 1–7.
21. Cademartiri, L.; Montanari, E.; Calestani, G.; Migliori, A.; Guagliardi, A.; Ozin, G. A. Size-Dependent Extinction Coefficients of PbS Quantum Dots. *J. Am. Chem. Soc.* **2006**, *128*, 10337–10346.
22. Moreels, I.; Justo, Y.; De Geyter, B.; Haustraete, K.; Martins, J. C.; Hens, Z. Size-Tunable, Bright, and Stable PbS Quantum Dots: A Surface Chemistry Study. *ACS Nano* **2012**, *5*, 2004–2012.
23. Jasieniak, J.; Bullen, C.; van Embden, J.; Mulvaney, P. Phosphine-Free Synthesis of CdSe Nanocrystals. *J. Phys. Chem. B* **2005**, *109*, 20665–20668.